

Metrology System for the Terrestrial Planet Finder Coronagraph

Stuart Shaklan¹, Luis Marchen, Feng Zhao, Robert D. Peters, Tim Ho, and Buck Holmes

Jet Propulsion Laboratory,
California Institute of Technology

ABSTRACT

The Terrestrial Planet Finder (TPF) employs an aggressive coronagraph designed to obtain better than $1e-10$ contrast inside the third Airy ring. Minute changes in low-order aberration content scatter significant light at this position. One implication is the requirement to control low-order aberrations induced by motion of the secondary mirror relative to the primary mirror; sub-nanometer relative positional stability is required. We propose a 6-beam laser truss to monitor the relative positions of the two mirrors. The truss is based on laser metrology developed for the Space Interferometry Mission.

1. INTRODUCTION

TPF Coronagraph (TPF-C) is a large, optical, space-based telescope scheduled to fly in 2015. It is designed to reduce scattered light from a target star to $< 1e-10$ of its peak intensity, enabling the detection of extra-solar terrestrial planets in reflected visible light appearing as close as 62 milli-arcseconds from the star. Ford et al review the mission and technical concepts¹.

The baseline design calls for an off-axis Cassegrain design with a 12 m focal length, elliptical 6 x 3.5 m primary mirror, and a secondary mirror ~ 10 m from the primary. The system focal length is 120 m. The coronagraph is placed behind the Cassegrain focus. The design, by P. Mouroulis, consists of collimating optics, a pair of deformable mirrors (DM), a fine-steering mirror, the coronagraph mask and Lyot plane, and all associated optics (Fig. 1).

The coronagraph is designed to provide better than $1e-10$ rejection of starlight and $2.5e-11$ stability of the rejected starlight inside the 3rd Airy ring, at $3 \lambda/D$, where λ is the wavelength (~ 600 nm) and D is the long dimension of the primary. This is a very aggressive design; working so close to the center of the image plane presents many difficulties, the most significant being the high sensitivity to changes in low-order aberrations. Green and Shaklan (2003) showed how various Lyot-type coronagraph designs exhibit low-order aberration sensitivity². Notably, pupil plane masks provide an alternative approach to the Lyot design with greatly reduced aberration sensitivity³, but the mask designs do not work at $3 \lambda/D$, requiring a larger telescope^{4,5} to allow detection of extra-solar terrestrial planets with operation at $> 4 \lambda/D$. The trade between aberration sensitivity and telescope size is under study by the TPF-C team at JPL.

In this paper we assume that a Lyot coronagraph is used. The specific coronagraph design calls for a radial $1-\text{sinc}^2(r)$ mask, with the radial coordinate scaled to match the elliptical shape of the image. This is one of a family of band-limited masks⁶, offering high diffraction rejection efficiency using hard-edged Lyot stops. The mask is scaled so that the first unity transmission peak (where $\text{sinc}(r)=0$) occurs at $4.5 \lambda/D$. The mask transmission at $3 \lambda/D$ is then 68% while the Lyot pupil efficiency is 32%⁷. We have chosen this mask because it offers high pupil plane efficiency and high image-plane throughput (\sim unity transmission beyond the first side-lobe). The linear $(1-\text{sinc}^2(x))$ form of this mask has been implemented with great success in the TPF High Contrast Test Bed⁸.

Our TPF model assumes a simple 'set-and-forget' scenario. The initial step is to measure the wave front and command the DM to compensate for all spatial frequencies within its control bandpass. The telescope is assumed to be stable in all respects during this time. When the science observation begins, thermal drifts, pointing errors, and reaction-wheel

¹ Contact information: Address: 4800 Oak Grove Drive, Pasadena, CA 91109. e-mail: Stuart.Shaklan@jpl.nasa.gov

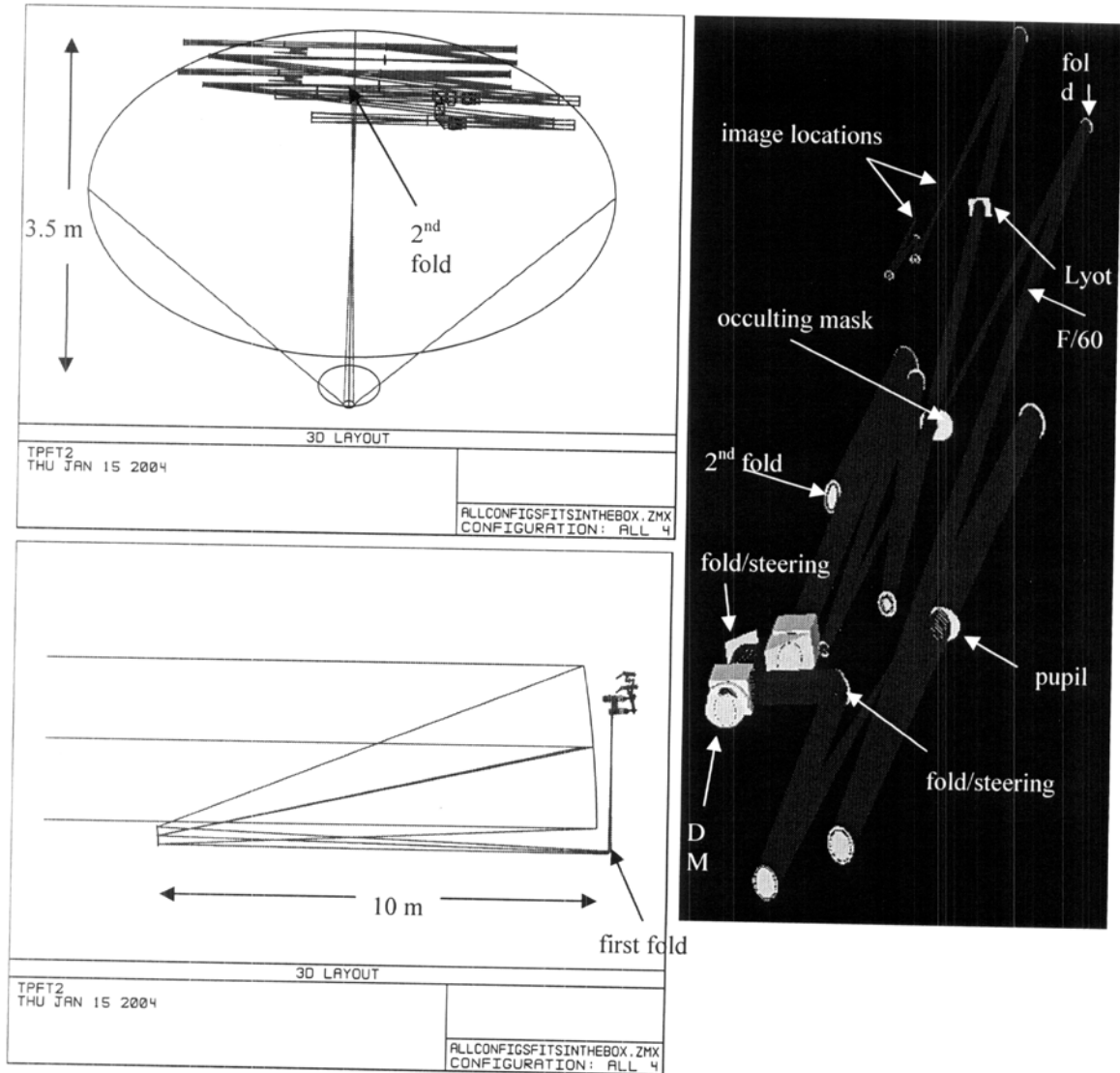


Figure 1. Optical layout of telescope and coronagraph.

induced jitter begin to affect the positions and shapes of the optics. No new wave front control command is issued until the system has deviated from its initial state by an amount specified in a detailed error budget.

One of the key terms in the error budget is the thermally induced motion of the secondary mirror relative to the primary. This motion changes focus, astigmatism, and coma content (and smaller amounts of higher-order aberrations as well). The motion tolerances, discussed in Sect. 2, are extremely tight.

In this paper, we propose to monitor the 6 degree-of-freedom (DOF) motions of the secondary mirror relative to the primary mirror using an infrared metrology system based on technology developed for the Space Interferometry Mission⁹ (SIM). The measurements can be used to control a set of actuators attached to the secondary, as well as for image post-processing. Our goal is to measure slow (< 1 Hz) motions with sufficient accuracy to enable control of secondary mirror motions for up to ~ 8 hours. The SIM technology does not provide sufficient sensitivity and bandwidth to control jitter-induced motions. These will be eliminated through design of isolation and damping mechanisms.

2. SENSITIVITY MODELS

Our modeling flow is depicted in Fig. 2. We use ray tracing to determine aberration sensitivity versus motion of the secondary mirror. We use a simple linear point-to-point model of the metrology beams to determine metrology beam length sensitivity to the 6 degree-of-freedom (6-DOF) motion of the secondary. These two models are combined to yield the aberration sensitivity versus metrology beam lengths. Finally, coronagraph model determines image plane

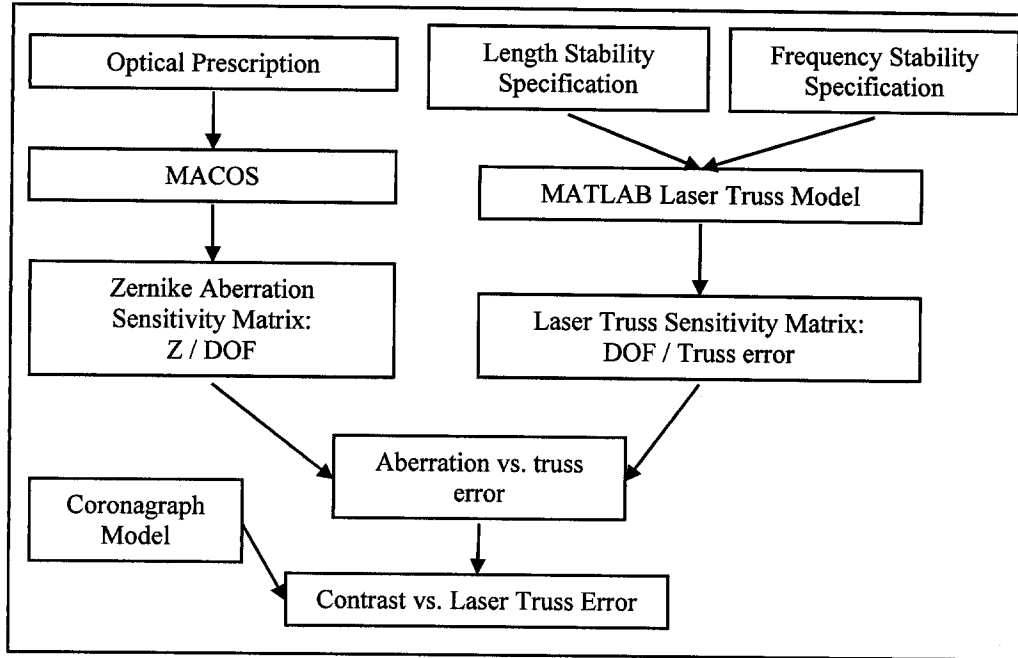


Figure 2. Modeling Flow Diagram.

contrast as a function of aberrations. We can thus determine by combining the linear and coronagraph models, the image plane contrast versus metrology beam length deviations.

The ray trace model employs the JPL-developed MACOS¹⁰ program driven by a MATLAB interface. MACOS reads the TPF-C optical prescription and traces a set of rays through the system. The system is traced in its nominal design state, then retraced for each of 6-DOFs of motion of the secondary mirror. The difference in the ray bundle from the nominal to perturbed state defines the change in aberration content for each DOF. With each perturbation, a fine-guiding mirror (FGM) is tilted to keep the spot centered on the mask. The FGM is located at a pupil-conjugate plane in the system upstream of the coronagraph mask. After the FGM, the beam follows the nominal design path. Thus all aberrations occur upstream of the mirror. By far the largest contributor is aberrations from the primary-secondary system, with negligible contributions related to the perturbed and displaced beam encountering other optics off-axis.

We represent the low-order aberrations with the first 15 Noll-ordered Zernike modes¹¹, stretched in one dimension to match the elliptical shape of the primary mirror. We chose a 30 cm grid spacing (compared to the 6 m long dimension of the primary) to provide adequate sampling for the aberrations. The first 15 Zernike modes are an adequate set, accounting for > 99% of the induced aberrations.

The metrology system is modeled as a set of six vectors, one per metrology beam. The six beams originate at the edge of the primary mirror at three points and intersect three points on the edge of the secondary, as shown in Fig. 3. The

geometry of the primary and secondary mirrors is taken from the optical prescription. The beam length sensitivity matrix is determined by moving the secondary in 6-DOFs just as for the aberration sensitivity matrix.

Two different metrology errors are modeled; random, uncorrelated errors, and laser frequency errors. The random uncorrelated errors enter by multiplying their variance (assumed to be the same for all beams) by the squares of the elements of the sensitivity matrix. This yields the variances of the 6-DOF motions of the secondary. Laser frequency errors have the effect of changing the scale of the beam. The associated length change is $L_i \Delta f / f$, where L_i is the length of the i th beam and $\Delta f / f$ is the relative frequency change. Given the relative frequency standard deviation, the 6-DOF standard deviations are determined by inner product of the beam length standard deviations with the sensitivity matrix elements (without squaring) since all the length changes are perfectly correlated.

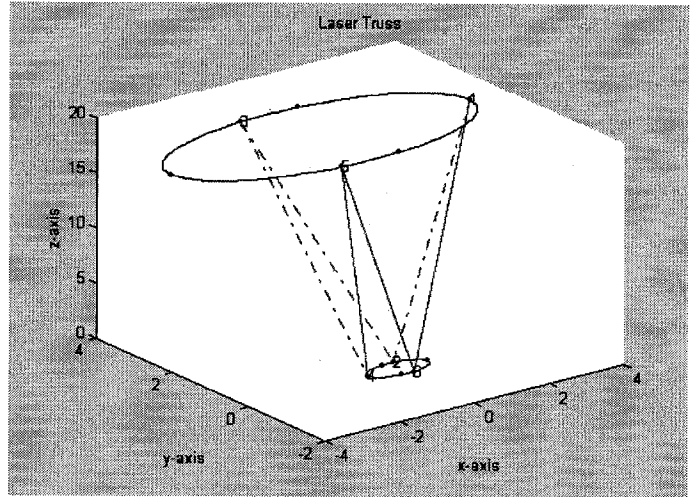


Figure 3. Metrology truss schematic. Units are m.

The coronagraph model has been described by Green and Shaklan (2003). Briefly, it assumes an ideal coronagraph mask placed in the image plane, and an ideal Lyot stop placed in the pupil plane, with perfect imaging between the planes. The model uses FFTs to compute the energy transmitted by the coronagraph for each of the first 15 Zernike modes. The model verifies the expected quadratic dependence of scattered energy on the aberration content for certain aberrations, and the quartic dependence on wave front tip/tilt.

3. PRIMARY-SECONDARY MIRROR MOTION REQUIREMENTS

The TPF-C error budget accounts for all the optical errors (wave front deformation, beam displacement on aberrated optics, aberrations caused by perturbations resulting in non-ideal states). The thermally induced motion of the secondary mirror, which we are concerned with here, accounts for just 6 of the hundreds of error budget terms (albeit 6 of the most important ones)! In addition to secondary mirror motion, there are ~ 10 critical optics, each with 6 DOF motion requirements and 15 wave front stability requirements (total of 21 DOFs per element), as well as two means of perturbation (thermal and jitter) per DOF.

The error budget contrast (intensity) terms are treated as uncorrelated and add linearly. The total error budget contrast stability specification is $2.5e-11$ to enable detection of planets with relative intensity of $1e-10$, with a signal-to-noise ratio of 4. Roughly speaking, this means that the scattered energy per speckle must be stable to a level of $2.5e-11$ of the energy collected from the target star. The scattered energy level has two contributions: time-variable terms mixing with static (set-and-forget) terms, and time-variable terms by themselves. Through a process whose description is beyond the scope of this paper, we have found that the time-variable terms must be limited to $7e-12$ to maintain overall stability of $2.5e-11$.

Of the $7e-12$ allocation, $8e-13$ is allocated to motion of the secondary mirror. This is split to $4e-13$ contrast contribution for random length errors and $4e-13$ for frequency stability errors. From these allocations, we can derive length and frequency stability requirements.

Table 1 gives the wave front aberration content and contrast contribution for Zernike modes 4-15. Mode 1 is inconsequential piston, while modes 2 and 3 are tip/tilt and are compensated by the FGM. As seen in column 3, only focus (mode 4) and coma (mode 8) make significant contrast contributions, even though the astigmatism wave front (modes 5,6) are of comparable magnitude. This is an artifact of our calculation, which is performed only at $3 \lambda/D$, on the

TABLE 1. Contrast Contributions from Metrology Length and Frequency Errors

Noll Zernike	Name	Random Length 217 pm r.m.s		Relative Freq. 3e-11 r.m.s.	
		Aberration (pm)	Contrast	Aberration (pm)	Contrast
4	Focus	1.78	3.13E-13	1.97	3.85E-13
5	Astigmatism	0.62	7.63E-25	0.04	1.61E-29
6	Astigmatism	1.01	5.41E-24	1.26	1.31E-23
7	Coma	0.18	1.63E-16	0.03	3.72E-18
8	Coma	0.36	1.03E-13	0.02	4.97E-16
9	Trefoil	0.16	3.57E-27	0.03	2.61E-30
10	Trefoil	0.17	1.20E-27	0.01	1.73E-32
11	Spherical	0.01	1.83E-17	0.01	1.83E-17
12		0.00	4.57E-17	0.01	7.38E-17
13		0.00	1.18E-18	0.00	4.49E-21
14		0.00	1.27E-33	0.00	1.30E-33
15		0.00	2.33E-34	0.00	5.23E-39
SUM			4.16E-13		3.85E-13

x-axis (parallel to the long axis of the primary mirror). This image point drives all the tolerancing; low order aberrations scatter less light at larger angles. Modes 5 and 6 do make contributions at other field points, but they are of diminishing importance as we move beyond 3 I/D.

We conclude from the modeling that random length errors are limited to 217 pm r.m.s. per beam, and the frequency stability is required to be $\Delta f / f = 3e-11$ r.m.s. These requirements apply for the full duration of the TPF measurement of a star, up to ~ 8 hours.

4. METROLOGY SYSTEM

4.1 Beam Launchers

At JPL we have been developing point-to-point metrology systems capable of meeting TPF length stability requirements (at least for ~ 1 hours time scales) for SIM⁹. Of particular interest is the architecture known as Common Path Heterodyne Interferometry (COPHI)¹². As with commercial systems, the metrology system architecture consists of a fiber-coupled heterodyne laser source and a fiber-fed beam-launcher head, with corner cubes defining the measurement end-points. In commercial systems, the beam-launcher head is placed between the corner cubes. In COPHI, the launcher is placed outside the cubes, and one cube has its vertex removed allowing the beam to pass to the second cube. The COPHI schematic is shown in Fig. 4 and the breadboard version built for SIM is shown in Fig. 5.

The COPHI architecture has several important advantages compared to commercial systems. It has very small non-common-path errors, which reduces thermal sensitivity. It relies on a wave front split rather than a polarization split, which reduces periodic (a.k.a. 'cyclic') error. Finally, with the corner cubes placed along the edges of the primary and secondary mirrors, the COPHI beam launchers do not block the starlight beam and they can be placed in the temperature-controlled isothermal cavity behind the TPF-C primary mirror (Fig. 6).

Variations of the COPHI configuration are used throughout the SIM internal and external metrology systems. They have been tested in high-precision testbeds and have been shown to perform to the TPF-C requirements, but only for short periods¹³ (chopping times are ~ minutes). Phase meter (electronic detection) performance has demonstrated Allan deviations of 10s of pm for 10,000 s. The limiting performance factors are related to thermal drift in the beam launcher internal and external alignment.

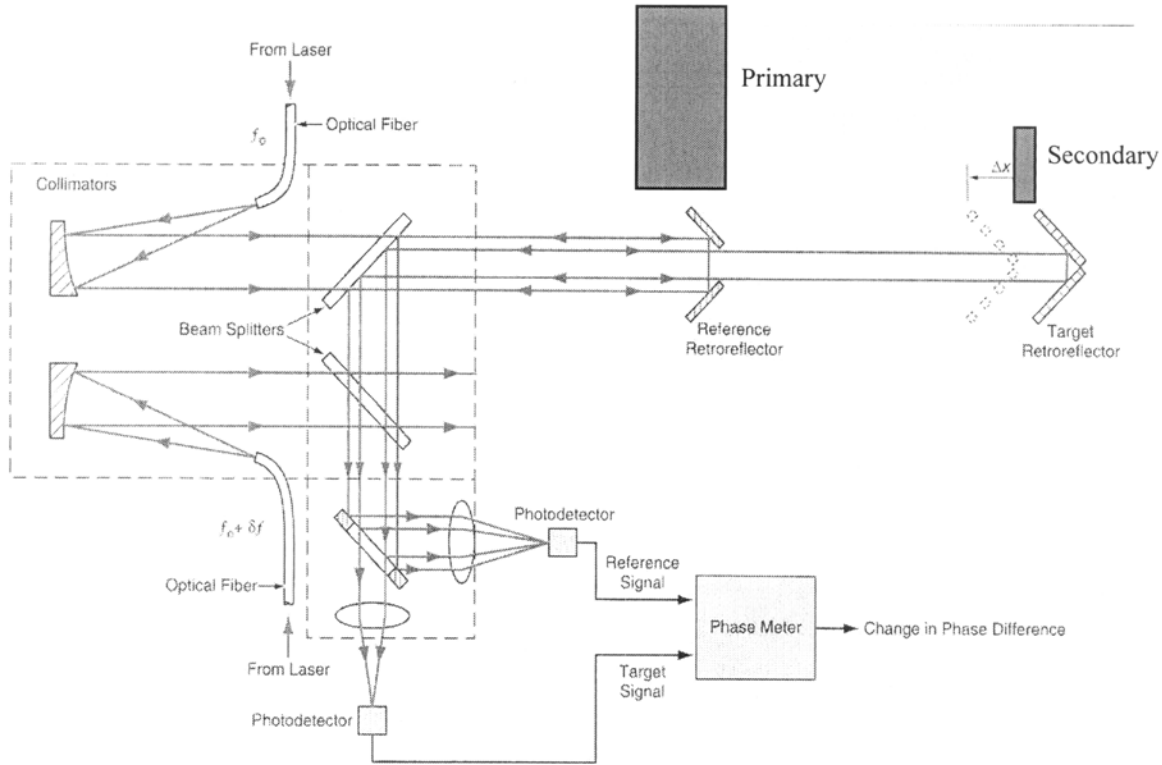


Figure 4. Schematic of COPHI beam Launcher. A single beam measures both the near and distant objects. A reference beam interferes with both return beams.

For TPF-C, the small angle between pairs of beams (see Fig. 6) will require some modifications to the SIM COPHI design to allow pairs of beam launchers to be oriented with their beams close to one another. This design change is not expected to significantly impact performance.

4.2 Corner Cubes

The open-faced corner cubes are attached around the outside of the primary secondary mirrors (Fig. 7). The cubes are made of three bonded pieces of ULE and will be required to have dihedral errors of ~ 1 arcsec. The cube attached to the primary mirror has a clear aperture of ~ 5 cm but it has no physical vertex; the cube still acts as a retroreflector but only for an annular beam. The 2 cm opening in the middle of the cube passes the inner part of the metrology beam to the smaller (~ 3 cm) cubes attached to the secondary mirror.

The most straightforward way to attach the cubes to the mirrors is to bond them directly to a small polished surface on the outer wall of the mirrors. Bulk thermal expansion of the bonding material will move the cube away from the mirrors but will induce negligible motion along the metrology beam direction. Creep along the surface of the optic should be $\ll 200$ pm during 8-hour observations.

We have analyzed launch-load stresses on the bond lines and have determined that they are below 700 psi. The model assumed a 200 g load applied parallel to the cube-mirror

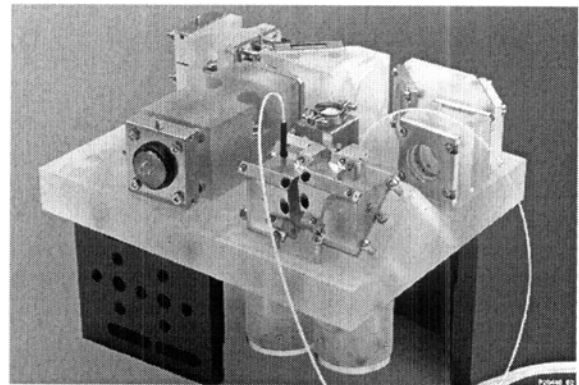


Figure 5. SIM breadboard version of COPHI.

interface. The maximum stress point occurs at the outer edge of the bond line between two of the corner cube prisms. Maximum stress along the cube/mirror interface is ~ 100 psi.

4.3 Pointing requirement

One potentially large source of metrology error is mispointing of the beam relative to the vector V connecting the two corner cube vertices. For a corner-cube based metrology measurement, one measures the vertex-to-vertex separation projected along the metrology beam, $L_m = |V| \cos(\theta)$, where θ is the angle between the beams, and L_m is the measured distance. For $|V|= 10$ m and a measurement error of 200 pm, this implies the beam direction must stay aligned to within ~ 1 arcsec of V . The stability requirement is tighter if there is a static offset. This challenging requirement appears in the SIM error budget as well and is addressed by modulating the beam direction to map out the measured distance versus angle¹⁴. An error signal is generated when the modulation is not centered on V . This approach has been successfully implemented in the SIM external metrology testbed¹⁵. One possible complication is that the dither, if too fast, introduces vibrations that can distort the primary mirror (an effect to which the coronagraph is exceedingly sensitive). The dither rate should be kept below the fundamental mirror and mount modes, typically > 10 Hz.

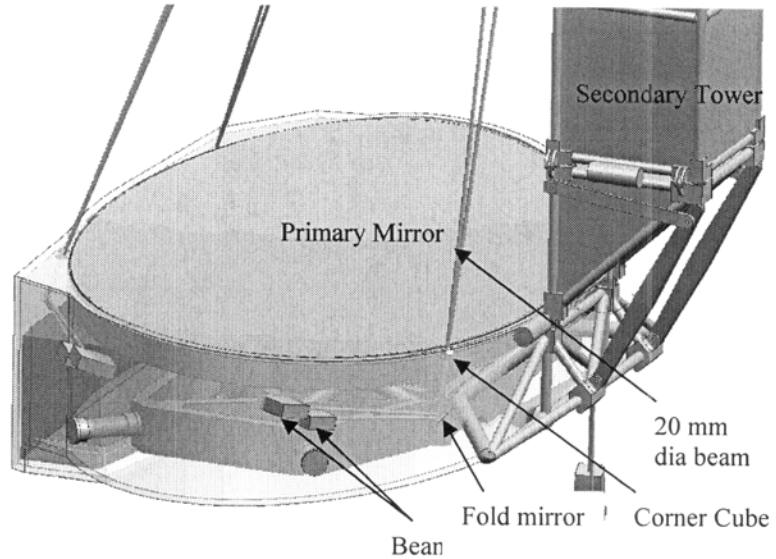


Figure 6. Metrology System Configuration. The area behind the primary mirror is an isothermal cavity controlled to room temperature.

4.4 Laser Source

In a heterodyne metrology system, the laser wavelength acts as the ruler we use to track the change in position of a target. Therefore, any change in laser wavelength during the course of a measurement will appear to the metrology system as if the target has moved. If the apparent target motion caused by laser frequency drift is larger than the required precision of the system, then the laser must be stabilized to an external frequency standard.

Given the target separation of 10m, the stability requirement for this application is 3×10^{-11} ($\Delta f/f$) for a measurement period of 8 hours. Additionally, the laser wavelength must be outside the response band of a silicon detector to not interfere with the science measurement. Therefore, the best wavelength of operation is either 1.319 μ m or 1.55 μ m. Very stable lasers have been made using monolithic non-planer ring oscillators (NPRO) of Nd:YAG at 1.319 μ m. However, these lasers still have a typical inherent stability on the order of 10^{-6} ($\Delta f/f$) over the 8-hour measurement period¹⁴. Distributed feedback diode lasers at 1.55 μ m also have comparable frequency stability. Therefore, an external frequency standard will be necessary to meet the requirement and due to development done by Space Interferometry Mission we will concentrate on the 1.319 μ m

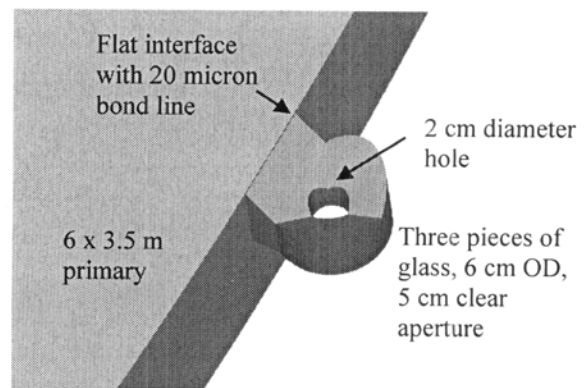


Figure 7. Corner cube mounted to edge of primary mirror.

Nd:YAG laser.

Much work has been done with Fabry-Perot etalons as an external laser frequency reference. These devices consist of two high reflectivity mirrors separated by some distance. They have a very narrow transmission band at regular intervals given as a function of the mirror separation. The locking technique most commonly used is an FM spectroscopy method developed by Pound-Drever-Hall¹⁵. Aside from the etalon, this technique requires only an electro-optic modulator and RF electronics and a detector operating in the few tens of megahertz. Laser stability based on these types of etalons has been reported at 10^{-11} ($\Delta f/f$) per day¹⁶, which would meet our requirements. However, since the frequency of the transmission peak depends on the mirror separation, the structure holding the mirrors must be made of a material with a low coefficient of thermal expansion and its temperature controlled very well to maintain stability.

Another option is to use an atomic or molecular resonance as a frequency standard. These standards have a couple key advantages over etalons. The primary advantage is the transitions are a physical property of the atom or molecule and do not drift as easily as the mirror spacing in an etalon. Another advantage is resonant frequency of most transitions are well known and documented. Therefore, by knowing which transition you are locked to, you know the absolute frequency of the laser which may or may not be needed depending on the metrology system.

Iodine is a common molecular reference for frequency stabilizing lasers due to the availability of usable transition lines in bands that can be probed either directly or by frequency doubling. The spectroscopy technique is very similar to the Pound-Drever-Hall method used on cavities with an electro-optic modulator and electronics operating at a few megahertz. The main difference is the optical layout. Since the iodine in the reference cell is gaseous, the transition line is Doppler broadened. To overcome this, counter-propagating pump and probe beams are used to lock to the Doppler-free molecules. This technique has been well documented with Nd:YAG lasers at $1.064\mu\text{m}$ doubled to 532nm , and is even available as a commercial system¹⁷ with frequency stability of 10^{-13} ($\Delta f/f$). There are also several iodine transition lines available to a doubled $1.319\mu\text{m}$ laser¹⁸, so we should be able to use a similar system to meet our requirements.

While iodine is a well-established frequency reference, it requires frequency doubling of the laser, which is a very inefficient process. Even with relatively high efficiency periodically polled frequency doublers, laser powers of several hundred milliwatts may be required and this would need to be considered in the design of a flight-qualified system. Methane, rubidium and other references may be an attractive alternative to iodine since they have lines that may be probed directly¹⁹, eliminating the high power required for frequency doubling. These references could be used in the same way as iodine, however they have not been as well investigated as laser frequency standards at $1.319\mu\text{m}$ and further testing should be done to verify their performance.

In summary, we have shown there are options for relative and absolute laser stability that have been shown to meet or exceed our requirements. There are no exotic components or electronics required for the stabilization system. Therefore, it is reasonable to conclude that a flight-qualified frequency stabilization system can be developed to meet these requirements without high risk to the project.

5. CONCLUSION

The TPF Coronagraph suffers no shortage of technical challenges. In this paper, we have defined the architecture of a metrology system that can be used to monitor one of the major sources of wave front error, thermally induced rigid-body motion of the secondary mirror relative to the primary mirror. The metrology requirements call for random length errors no greater than 217 pm r.m.s , and relative frequency stability of at least $3\text{e-}11$, for periods up to 8 hours.

By the time TPF-C flies, the Space Interferometry Mission will have completed its primary mission using a high precision heterodyne metrology system that comes close to meeting the TPF-C requirements. The SIM launchers have stability requirements that apply on time scales of 30 s to 1 hour, about an order of magnitude shorter than the TPF-C requirements. There is no stringent frequency stability requirement on SIM. Also, the SIM configuration does not require that pairs of beams be launched within close proximity as required for TPF-C. Some development is required, however much can be inherited from SIM and we are confident that over the next several years, additional development will enable the proposed metrology system will meet the TPF-C requirements.

ACKNOWLEDGEMENTS

We wish to acknowledge the technical contributions of Joseph Green, Pantazis Mouroulis, and Scott Basinger to this body of work. This work was carried out at the Jet Propulsion Laboratory, California Institute of Technology, under contract with the National Aeronautics and Space Administration.

REFERENCES

1. Ford, V.G., et al, "The Terrestrial Planet Finder Coronagraph," Proc. SPIE Vol. 5170, pp. 1-12 (San Diego, 2003).
2. Green, J.J., and Shaklan, S.B., "Optimizing Coronagraph Performance Designs to Minimize Their Contrast Sensitivity to Low-Order Optical Aberrations," Proc. SPIE Vol. 5170, pp. 25-37 (San Diego, 2003).
3. Green, J.J., and Shaklan, S.B., "The Sensitivity of Shaped Pupil Coronagraphs to Optical Aberrations," Proc. SPIE (Glasgow, 2004, to be published).
4. Kasdin, N.J., Vanderbei, R.J., Spergel, D.N., Littman, M.G., "Extrasolar planet finding via optimal apodized-pupil and shaped-pupil coronagraphs," ApJ 582, pp. 1147-1161 (2003).
5. Vanderbei, R.J., Spergel, D.N., & Kasdin, N.J., "Circularly Symmetric Apodization via Star-shaped Masks," ApJ 599, pp. 686-694 (2003).
6. Kuchner, M.J., and Traub, W.A., "A Coronagraph with a Band Limited Mask for Finding Terrestrial Planets," ApJ 570, pp. 900-908 (2002).
7. Green, J.J., private communication, 2003.
8. Green, J.J. et al, "Demonstration of Extreme Wavefront Sensing on the TPF High-Contrast Imaging Testbed," Proc. SPIE, Vol. 5170, pp. 38-48 (Waikoloa, 2002).
9. Laskin, R.A., "SIM Technology Development: Light at the End of the Tunnel," SPIE Vol. 4852, pp. 16-32 (Waikoloa, 2002).
10. MACOS (Modeling and Analysis of Controlled Optical Systems) Manual, JPL Document.
11. Noll, R.J., "Zernike Polynomials and Atmospheric Turbulence." J. Opt. Soc Am., vol. 66, pp. 207-211 (1976).
12. Zhao, F., et al, "SIM Internal Metrology Beam Launcher Development," Proc. SPIE Vol. 4852, pp. 370-379 (Waikoloa, 2002).
13. Nemati, B., "External Metrology Truss Technology Demonstration (KITE)," Proc. SPIE Vol. 4852, pp. 90-99 (Waikoloa, 2002).
14. Lightwave Electronics Corp. model 125 specifications.
15. R.W.P. Drever, J. L. Hall, F. V. Kowalski, J. Hough, G. M. Ford, A. J. Munley, and H. Ward, "Laser Phase and Frequency Stabilization Using an Optical Resonator", *Appl. Phys. B*, 31, 97 (1983).
16. <http://www.npl.co.uk/length/projects/pt9915.html>
17. Email correspondence with Innolight.
18. A. Arie, et al, "Iodine spectroscopy and absolute frequency stabilization with the second harmonic of the 1319-nm Nd:YAG laser", *Opt. Lett.*, 18 p. 1757 (1983)
19. T. Dennis, et al., "Wavelength References for 1300-nm Wavelength-Division Multiplexing", *J. Lightwave Technol.*, 20 p. 804 (2002)